Proceedings of the 2012 IEEE 12th International Conference on Bioinformatics & Bioengineering (BIBE), Larnaca, Cyprus, 11-13 November 2012

An Image-based Method for Quantification of Lateral Pterygoid Muscle Deformation

Yang Yang[1,2], Kelvin Weng Chiong Foong[1,2], Sim Heng Ong[1,3,4], Masakazu Yagi[5], Kenji Takada[2,6]
[1]NUS Graduate School for Integrative Sciences and Engineering, National University of Singapore
[2]Faculty of Dentistry, National University of Singapore
[3]Department of Electrical and Computer Engineering, National University of Singapore
[4]Department of Bioengineering, National University of Singapore
Singapore 119083, Singapore
[5]The Center for Advance Medical Engineering and Informatics, Osaka University
[6]Department of Orthodontics and Dentofacial Orthopedics, Graduate School of Dentistry, Osaka University
Osaka 5650871, Japan
Email: yang01@nus.edu.sg

Abstract—**The aims of this study were to present a method quantifying and visualizing the deformation of subject-specific lateral pterygoid muscles (LPM) during a simulated jaw-opening movement. A normal adult male subject underwent magnetic resonance (MR) scans of the head at three mandibular positions: mandibular rest (M0), medium jaw-opened (M1), and maximum jaw-opened (M2) positions. The 3D models of the LPM were reconstructed from the three sets of MR images. The deformations of each muscle in the two cases (M0→M1 and M1→M2) were quantified in terms of the displacements of region correspondences between the muscle models before and after the mandibular position changed. The 3D models of the subject-specific LPM were reconstructed, and the directions and magnitudes of deformations of each muscle in the two cases were accurately quantified and visualized in the three anatomic planes. The functional activities along the entire body and at specific compartments of subject-specific LPM were quantified and visualised using the quantified 3D deformations of the LPM as a new descriptor. The presented method defined the deformations of the subject-specific LPM, and revealed the anatomic architectural and biomechanical characteristics of the subject-specific LPM appropriately and meaningfully in the simulated jaw-opening movement.**

Keywords: Lateral pterygoid muscles, deformation, mandibular movements, functional roles, magnetic resonance image.

I. INTRODUCTION

Studies of functional activities of lateral pterygoid muscles (LPM) have an important bearing on two clinical situations which are to clarify the functional roles of LPM in mastication and to explain problems associated with temporomandibular joint (TMJ) [1]. The electromyographic approach (EMG) for the studies of LPM has been widely accepted. For example, Gibbs et al [2] and Wood et al [3] revealed that the inferior head and superior head of LPM have different functional roles during jaw-closing and jaw-opening. However Hannam and McMillan [4] and Ruangsri et al [5] have suggested that the two heads of LPM should be regarded as a single muscle. The major reason for the differing conclusions was the inability of previous studies to verify whether the EMG recording electrodes were correctly located within the muscle, as suggested by Murray et al [6]. Moreover, Hiraba et al [7] suggested that the superior head controlled the angular relationship between the articular disk and the condyle. On the other hand, a series of recent studies employing medical imaging [8, 9] attempted to explain the functional roles of the LPM by using the dimensional parameters such as the changes in muscle volume, length and cross-sectional areas (CSAs) when the mandible moved from the intercuspal position to the maximum jaw-opened position. Although the EMG approach promoted a large number of investigations in the functional roles of the LPM as used often in mastication and in TMJ function studies, the normal functional roles of LPM in mastication remain unclear. Moreover studies using the dimensional parameters of a muscle are not suited to describing the functional roles of the LPM meaningfully. Hence, the aims of this study were to quantify and visualize the deformations of subject-specific LPM in a simulated jaw-opening movement for studying their functional roles in mastication and TMJ function.

II. MATERIAL & METHOD

A. Image Data Acquisition

Three significant mandibular positions were selected to simulate a successive jaw-opened movements: (1) mandibular rest position (M0); (2) medium jaw-opened position (M1), which is the mid-position between the M0 and the maximum jaw-opened position (M2); and (3) M2 achieved by each subject's effort as the maximal vertical mouth opening without

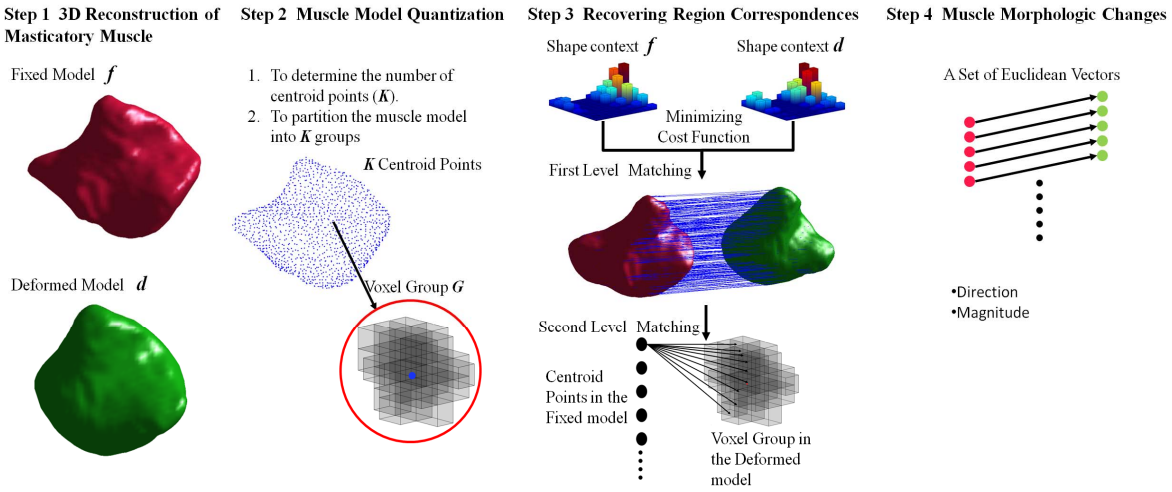

Figure 1. Quantification of Muscle Deformation

pain or discomfort. To ensure a stable relationship of the teeth at M0, M1 and M2 during the MR scans, three acrylic bite props were customized for the subject. A normal adult male subject (31 years of age, without any dental problems in clenching and jaw-opened movements) underwent MR scans of the head with the mandible at the four positions, with each scan lasting five minutes. The protocol (T1 pulse sequence; echo time (TE): 5 ms; repetition time (TR): 11.1 ms; slice thickness: 0.7 mm; spatial resolution: 0.7 mm, 1 mm, 1 mm) was carried out with a 1.5 Tesla MR scanner (Signa HDx 1.5T, General Electric, Harvey, IL, USA). After the MR scans, the four sets (M0, M1, M2 and M3) of the whole-head MR images were registered by MedINRIA-ImageFusion software (INRIA, France).

B. *Quantification of Muscle Deformation*

The deformations of the subject-specific LPM in the two cases (i.e., M0→M1 and M1→M2) were quantified according to the next four steps as Fig. 1 shows.

1) Three-dimensional reconstruction of lateral pterygoid muscle: the LPM of the subject were semi-automatically segmented from the three sets of MR images by ITK-SNAP (http://www.itksnap.org). The inter-rater reliability and the intra-rater reliability of the six muscle segmentations (the left and right muscles at the three mandibular positions) were assessed by the comparisons of the muscle volumes between occasions and between raters using the intraclass correlation coefficient (ICC) as described in [10].

2) Muscle Model Quantization: To numerically describe the 3D morphology of each muscle model and compute region correspondences between the two 3D muscle models (i.e., the fixed model and the deformed model shown in Fig. 1 Step 1) before and after mandibular position changed in each case in Step 3, the large set of voxels in each model was partitioned into specific groups having approximately the same number of voxels nearest to them, and each group was represented by its centroid point (Fig. 1 Step 2). The Lloyd algorithm [11] was employed to achieve the muscle model quantizations.

3) Recovering region correspondences: The original shape context method [12] is a shape feature descriptor that allows for measuring shape similarity and the recovering of point correspondences in 2D case, and then extended for 3D case by [13]. To reduce local errors between the locations of its recovered corresponding points and their exact corresponding points in the fixed model, the original shape context was modified to be a double matching algorithm (Fig. 1-Step 3) described in the next four steps:

a) Compute the 3D shape context for each muscle model using the centroid points obtained in Step 2 by (1).

$$h_{1\le i\le K}(m,n)=\#\{q\neq p_i:(q_{x,y}-p_{i(x,y)})\in bin(m),\ (q_{y,z}-p_{i(y,z)})\in bin(n)\} \quad (1)$$

where $h(m,n)$ is the 3D shape context descriptor for each muscle model. p_i is the i^{th} centroid point obtained, and q are the remaining $K-1$ centroid points in the muscle model. m and n indicate a spherical coordinate system (m: 12 bins in horizontal plane, n: 6 bins in vertical plane). x, y, z are the Cartesian coordinates of each centroid point in the muscle model.

b) Compute all possibilities of the corresponding relations between the fixed model and the deformed model by (2). $f(m,n)$ and $d(m,n)$ are the 3D shape context descriptors for the fixed model and the deformed model, respectively.

$$C_S=\frac{1}{2}\sum_{i=1}^{m}\sum_{j=1}^{n}\frac{(d(m,n)-f(m,n))^2}{d(m,n)+f(m,n)} \quad (2)$$

c) Find the first level corresponding relation between the two models by minimizing the cost function C_S using Hungarian method [14].

d) Compute the second level corresponding relation: in c), the first level corresponding relation is obtained. e.g., the centroid point C_{f_i} in the fixed model corresponds to C_{d_j} in

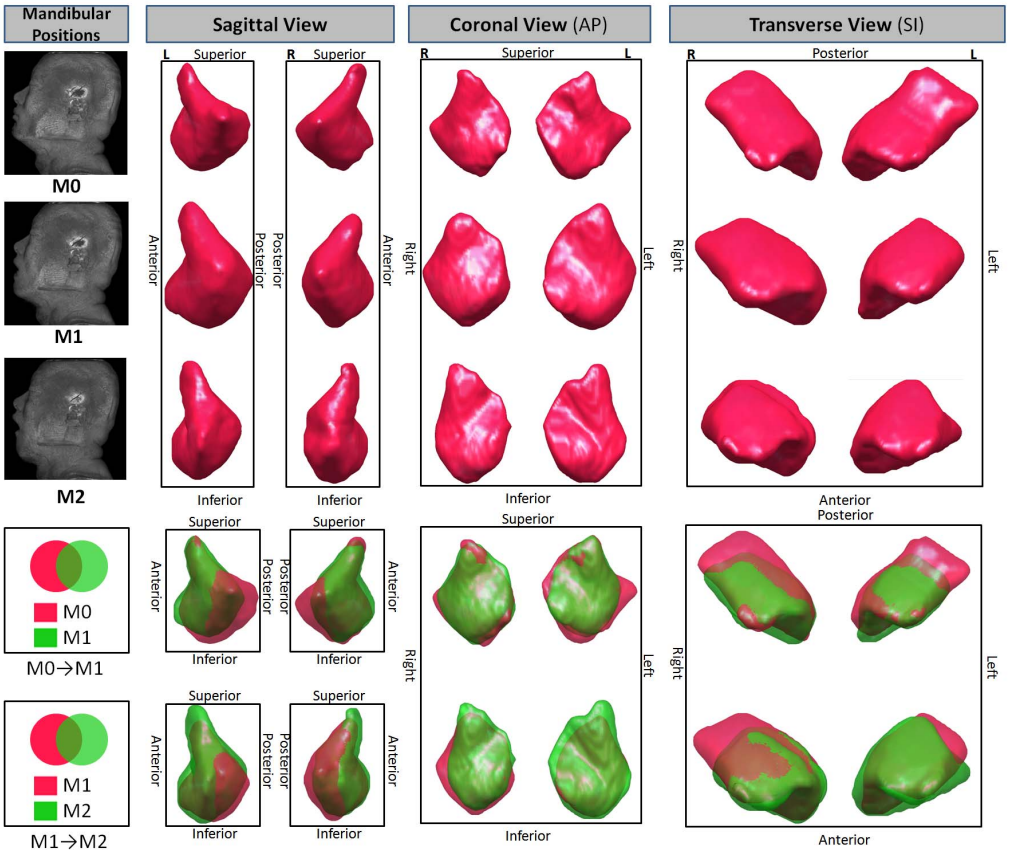

Figure 2. Three-dimensional reconstruction of lateral pterygoid muscles. AP: from anterior to posterior; SI: from superior to inferior; 'L' and 'R' indicate the left and right sides, respectively

the deformed model. But there may be an error between the locations of C_{d_j} and its exact corresponding point for the centroid point C_{f_i} since the two do not necessarily coincide. To reduce this error, the shape context descriptor of each voxel centroid P_i in the group G_j represented by C_{d_j} was calculated with the other centroid points in the deformed model by (3).

$$P_i(m,n) = \#\{C_{d_n} \neq C_{d_j} : (C_{d_{n(x,y)}} - p_{i(x,y)}) \in bin(m), \\ (C_{d_{n(y,z)}} - p_{i(y,z)}) \in bin(n)\} \quad (3)$$

where P_i and $P_i(m,n)$ are the i^{th} voxel centroid in the group G_j and its shape context descriptor. C_{d_n} are the centroid points in the deformed model except C_{d_j} The second level corresponding relation was then determined by $\arg\min_{1\le i\le v} \| P_i - f_j \|^2$ as finding the voxel centroid P_i having the most similar shape context descriptor with C_{f_i} in the group G_j. f_j is the shape context descriptor of the C_{f_i} and v is the number of voxels in the group G_j.

4) Muscle deformation field: After recovered the region correspondences between the fixed model and the deformed model, a set of Euclidean vectors which denote the displacements between pairs of corresponding points was obtained as shown Fig. 1-Step 4. The direction and magnitude of each Euclidean vector was used to describe the muscle deformation from the fixed model to the deformed model in each case, and the resultant direction of the set of Euclidean vectors could be used to indicate the direction of the muscle tension.

III. Experiments & Results

A. Three-dimensional reconstruction of lateral pterygoid muscles.

A total of six 3D muscle models under the three mandibular positions were reconstructed. The two models before and after mandibular position changed in each case were demonstrated in the same coordinate system by different colors as Fig. 2 shows. The intra-rater reliability and inter-rater reliability of the segmentations of the six muscles were very high, with ICC of 0.990 and 0.982, respectively. The deformations of the LPM accompanied by the changes of mandibular position were clearly seen from these reconstructed muscle models, moreover the differentials of the deformations between the left and right muscles were also observed.

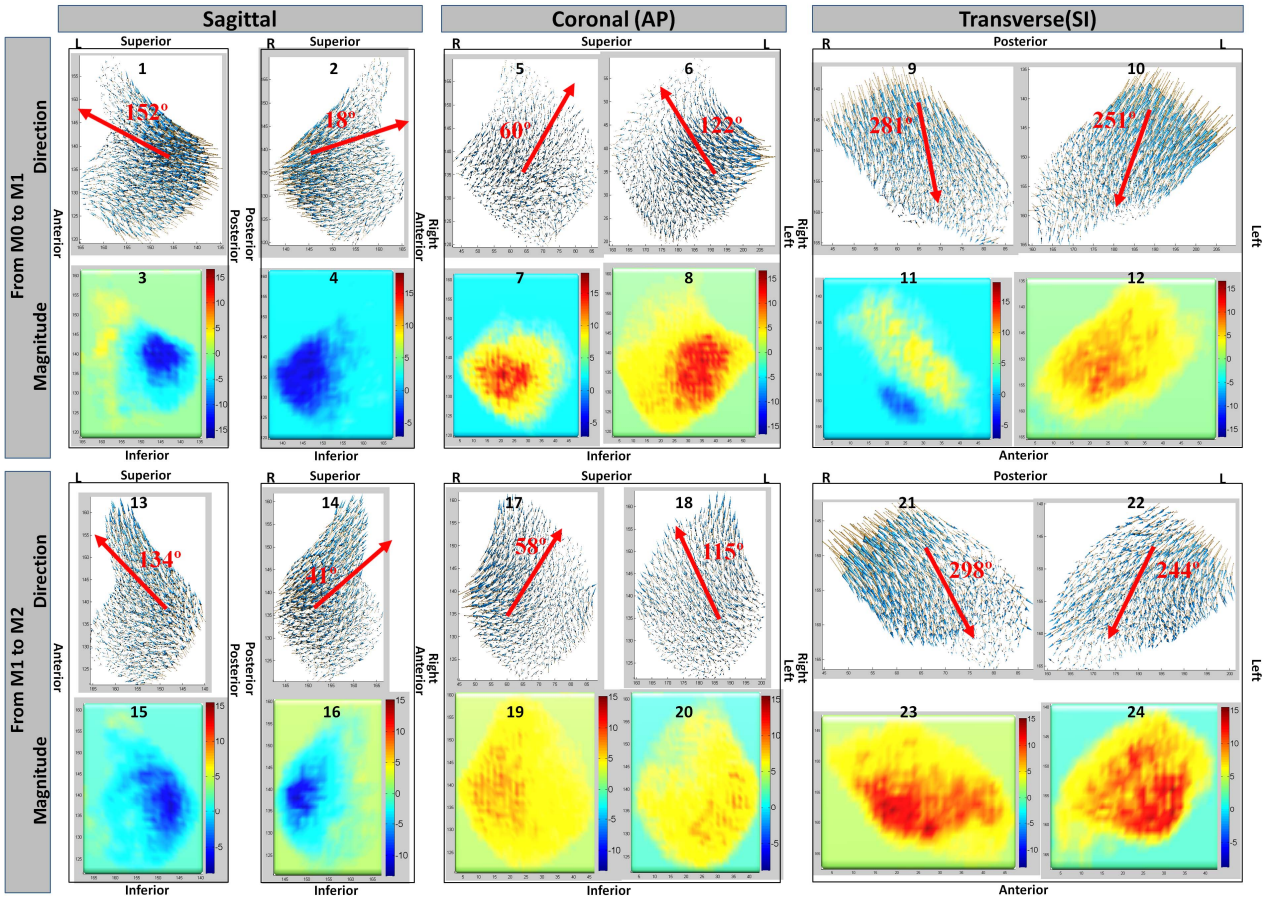

Figure 3. Deformations of lateral pterygoid muscles in the two cases. In 'Direction' rows, the direction of each centroid point displacement is indicated by a 3D arrow (blue) in the three anatomic planes, respectively, and the size of each 3D arrow represents the magnitude of each centroid point displacement. The 2D arrows (red) indicate the resultant directions of displacements of all centroid points in the three planes, respectively. In 'Magnitude' rows, the displacements of all centroid points in each case were decomposed into the three anatomic planes, respectively, and the color maps show the magnitudes of the decomposed displacements. The positive and negative values in the color maps denote the morphologic changes in the outward and inward directions, respectively. L: left side; R: right side; AP: from anterior to posterior; SI: from superior to inferior. These results were computed by 1500 centroid points and demonstrated by using MATLAB (MathWorks, U.S.A).

B. Validation of non-rigid point matching

The proposed method can be classified as a geometric feature based non-rigid point matching which can be used for non-rigid registration. In non-rigid registrations, the thin plate spline (TPS) transformation is commonly applied for the coordinate transformations after the correspondences between two objects determined, and its performance is mainly determined by the accuracy of the recovered correspondences [12], i.e., an incorrect correspondence would misguide the TPS transformation leading to unacceptable results. In this study, the 3D TPS transformation was employed to generate a simulated muscle model M_T by the recovered correspondences , and the accuracy of the non-rigid point matching was validated through the geometric similarity comparisons between the simulated muscle model M_T and the original muscle model M_O (reconstructed in II-B-1) by using the two parameters: symmetric mean absolute distance (SMAD) and Hausdorff distance (HD) [15]. The results are shown in Table 1. As expected, the point matching using 1500 centroid points performed better results, i.e. HD: 3.95 (0.13), SMAD: 0.515 (0.006). The global errors in terms of HD and SMAD were reduced by increasing the numbers of control points from 500 to 1500. The reason is that the approximation of the continuous muscle could be improved and the local error between the locations of its recovered corresponding point and its physically exact corresponding point could also be reduced when the number of centroid points increases.

Table 1. Validation of the proposed method

Number of points (Npnts), Hausdorff distance (HD), Symmetric mean absolute distance (SMAD), Mean (standard deviation) as computed from the four cases of muscle deformations. 1: left muscle M0→M1; 2: left muscle M1→M2; 3: right muscle M0→M1; 4: right muscle M1→M2

		Case				
Npnts	Parameters	1	2	3	4	Mean (SD)
500	HD [LPM]	5.8	6.5	5.9	6.3	6.13(0.33)
	SMAD[LPM]	0.62	0.62	0.61	0.61	0.615(0.006)
1000	HD[LPM]	4.6	4.9	4.8	5.0	4.83(0.17)
	SMAD[LPM]	0.55	0.55	0.55	0.56	0.553(0.005)
1500	HD[LPM]	3.8	4.1	3.9	4.0	3.95(0.13)
	SMAD[LPM]	0.52	0.52	0.51	0.51	0.515(0.006)

C. Muscle deformation fields

According to the validation results in B, 1500 centroid points were employed to quantify the deformations of the LPM in this study. The quantified muscle deformation fields were visualized in the three anatomic planes in Fig. 3. In the first case (M0→M1): the LPM on both sides contracted anteriorly and superiorly (Fig. 3–1&2), and constricted inwardly (Fig. 3-3&4) in the sagittal plane; in the coronal plane, the LPM on both sides contracted to superior and medial (Fig. 3-5&6), and bulged anteriorly (Fig. 3-7&8); in the transverse plane, the LPM on both sides contracted to anterior and medial (Fig. 3-9&10), and bulged superiorly (Fig. 3-11&12). In the second case (M1→M2): in the sagittal plane, the LPM kept contracting anteriorly and superiorly (Fig. 3-13&14), and the regions constricting inwardly (Fig. 3-15&16) were larger than the regions (Fig. 3-3&4) in the first case; in the coronal plane, the LPM kept contracting to superior and medial (Fig. 3-17&18). The muscles on both sides kept bulging anteriorly (Fig. 3-19&20), but the region bulging anteriorly in the right muscle became larger comparing with the first case; in the transverse plane, the LPM kept contracting to anterior and medial (Fig. 3-21&22). The muscles on both sides kept bulging superiorly (Fig. 3-23&24), but the region bulging superiorly in the right muscle became larger. According to the calculated resultant directions of the 3D morphologic changes of the LPM in the two cases, the LPM contracted more superiorly and medially in the second case (i.e. 134º<152º in Fig. 3-1&13 and 41º >18º in Fig. 3-2&14; 298º>281º in Fig. 3-9&21 and 244º <251º in Fig. 3-10&22). Moreover the muscle deformations in the insertions of the LPM were larger than the deformations in other regions (i.e. the 3D arrows in the insertions of the LPM had bigger sizes in Fig. 3 'Direction' rows).

IV. Discussion

This study appropriately and meaningfully describes the anatomic architectural and biomechanical characteristics of the subject-specific LPM using the quantified deformation fields of the subject-specific LPM as compared with previously published muscle dimensional parameters such as volume, CSAs and thickness. The exact functional roles of the entire muscle and the specific muscle compartments can also be effectively evaluated by the present method. Despite the present methodological limitation, i.e., the three stepwise mandibular positions were used to simulate a successive mandibular movement, future work could involve real time MR imaging of the movements of masticatory muscles since such a technique has been already used experimentally [16]. We believe that future studies using the present method with larger samples would be helpful to clarify the functional roles of the superior and inferior heads of LPM, and further explain the functional roles of LPM in mastication and TMJ functions. Furthermore the present method could possibly be used to identify the aetiology of temporomandibular joint disorder (TMJD) for different individuals.

Acknowledgment

This project had been funded by the Singapore Bio-Imaging Consortium. The authors wish to thank the Global Centers of Excellence Program, Japan, for supporting the research collaboration between the National University of Singapore and Osaka University.

References

[1] J.P. Lund, G.J. Lavigne, R. Dubner and B.J. Sessle. "Orofacial pain; from basic science to clinical management," Chicago, Quintessence Publ. Co, 2001.

[2] C.H. Gibbs, P.E. Mahan, T.M. Wilkinson and A. Mauderli. "EMG activity of the superior belly of the lateral pterygoid muscle in relation to other jaw muscles," *J Prosthet Dent*, vol. 51, pp. 691-702, 1984.

[3] W.W. Wood, K. Takada and A.G. Hannam. "The electromyographic activity of the inferior part of the human lateral pterygoid muscle during clenching and chewing." *Arch Oral Biol*, vol. 31, pp. 245-253, 1986.

[4] A.G. Hannam and A.S. McMillan. "Internal organization in the human jaw muscles," *Crit Rev Oral Biol Med*, vol. 5, pp. 55-89, 1994

[5] S. Ruangsri, T. Whittle, K. Wanigaratne and G.M. Murray. "Functional activity of superior head of human lateral pterygoid muscle during isometric force," *J Dent Res,* vol. 84, pp. 548-553, 2005.

[6] G.M. Murray, I. Phanachet, S. Uchida and T. Whittle. "The human lateral pterygoid muscle: A review of some experimental aspects and possible clinical relevance," *Aus Dent J*, vol. 49, pp. 2-8, 2004.

[7] K. Hiraba, K. Hibino, K. Hiranuma and T. Negoro. "EMG activities of two heads of the human lateral pterygoid muscle in relation to mandibular condyle movement and biting force," *J Neurophysiol,* vol. 83, pp. 2120-2137, 2000.

[8] T.K. Goto, K. Tokumori, Y. Nakamura, M. Yahagi, K. Yuasa, K. Okamura and S. Kanda. "Volume changes in human masticatory muscles between jaw closing and opening," *J Dent Res,* vol. 81, pp. 428–432, 2002.

[9] T.K. Goto, M. Yahagi, Y. Nakamura, K. Tokumori, G.E. Langenbach and K. Yoshiura. "In vivo cross-sectional area of human jaw muscles varies with section location and jaw position," *J Dent Res*, vol. 84, pp. 570–576, 2005.

[10] D. Maret, F. Molinier, J. Braga, O.A. Peters, N. Telmon, J. Treil, J.M. Inglese, A. Cossie, J.L. Kahn and M. Sixou. "Accuracy of 3D reconstructions based on cone beam computed tomography," *J Dent Res*, vol. 89, pp. 1465-1470, 2010.

[11] S.P. Lloyd. "Least squares quantization in pcm," *IEEE Trans. Inf. Theory*, vol. 28, pp. 129–137, 1982.

[12] S. Belongie, J. Malik and J. Puzicha. "Shape matching and object recognition using shape contexts," *IEEE Trans. Pattern Anal. Mach. Intell*, vol. 24, pp. 509-522, 2002.

[13] M. Kortgen, G.J. Park, M. Novotni and R. Klein. "3D shape matching with shape context," *In Proc of The 7th Central European Seminar on Computer Graphics*, Budmerice, Slovakia, 2003.

[14] H.W. Kuhn. "The Hungarian method for the assignment problem," *NAV RES LOGIST Q*, vol. 2, pp. 83–97, 1955.

[15] K.O. Babalola, B. Patenaude, P. Aljabar, J. Schnabel, D. Kenedy, W. Crum, S. Smith, T. Cootes, M. Jenkinson and D. Rueckert. "An evaluation of four automatic methods of segmenting the subcortical structures in the brain," *Neuroimage*, vol. 47, pp. 1435-1447, 2009.

[16] S. Zhang, K.T. Block and J. Frahm. "Magnetic resonance imaging in real time: advances using radial FLASH," *J Magn Reson Imaging*, vol. 31, pp. 101-109, 2010.